AIAA SciTech Forum
8-12 January 2024, Orlando, FL
AIAA SCITECH 2024 Forum

10.2514/6.2024-0925

Initial Radical Oxygen Concentration Measurements Using Catalytic Probes in an RF Plasma

Alexandra N. Leeming *, Allison E. Timm †, and Joshua L. Rovey ‡
University of Illinois Urbana-Champaign, Urbana, Illinois, 61801

Michael McDonald§
United States Naval Research Laboratory, Washington, DC 20375, United States

Electric propulsion (EP) systems are vital for space exploration and satellite station keeping. Traditionally, xenon has been the preferred propellant for these systems due to its high mass efficiency and performance. However, its growing demand and limited supply have driven the need to explore alternative propellants. These alternative propellants pose challenges, particularly the generation of reactive species, such as radical oxygen neutrals, which can significantly degrade spacecraft components and affect the operational lifetime of EP systems. This study uses a radio-frequency (RF) oxygen plasma to generate radical oxygen neutrals for catalytic probe development for the validation of catalytic probe use in determining atomic oxygen density measurements in future EP systems. This was done by employing nickel catalytic probes to characterize the atomic neutral density over a power range of 10 to 600 W within an RF plasma. The average atomic neutral density measured in the RF plasma source ranged from 6.1×10^{18} m^{-3} to 3.8×10^{20} m^{-3} over the RF power range. Furthermore, this investigation presents a comparative analysis of 99.9% pure nickel and 98.9% shim nickel as catalytic surfaces. The results reveal an average of 18% difference between the atomic oxygen neutral density measured by the pure and shim nickel. These results suggest that catalytic recombination is sensitive to material properties indicating that minor variations in purity can influence recombination rate and probe temperature. This study demonstrates that catalytic probes are a promising approach for measuring atomic oxygen neutral densities in EP systems.

I. Introduction

Electric propulsion (EP) utilizes electric and magnetic fields to ionize and accelerate propellant. This process increases the propellant's exhaust velocity, imparting momentum to the spacecraft. EP systems primarily utilize gas propellants as they are easily ionized and accelerated by electric and magnetic fields [1]. Xenon is the most commonly used propellant in EP systems due to its low ionization potential, high density, and chemical inertness [1]. However, xenon is expensive and in short supply. There is a growing demand for it beyond EP applications, in areas such as medical anesthesia and automotive lighting [2]. Due to these factors, along with supply shocks during the COVID-19 pandemic and the Ukraine invasion, recent work has concentrated on finding alternative propellants for EP systems [2–5]. Efforts have focused on three main categories of propellants: gaseous, condensed, and molecular. Gaseous propellants include noble gases such as krypton, argon, and neon [3]. Condensed propellants are solids or liquids at room temperature and encompass metals such as bismuth, iodine, and zinc [2, 4]. However, molecular propellants, such as oxygen, nitrogen, carbon dioxide, and water (also condensable) have garnered the most interest over recent decades due to their wide availability, low toxicity, and low price point [2].

One major challenge facing the integration of alternative propellants in EP systems is cathode poisoning. Poisoning occurs when chemical reactions take place in the pores of the thermionic insert, creating deposits that decrease the ability of the insert to provide electrons [1]. The presence of these deposits elevates the work function of the insert which leads to inconsistent electron emission and a reduction in cathode lifetime. As a result, the thermionic insert does not efficiently produce electrons, adversely affecting the overall performance of the thruster [6]. Previous studies have demonstrated that cathode poisoning is most prevalent due to oxygen, water, carbon dioxide, and air [7]. This presents a

*Graduate Research Assistant, Aerospace Engineering, AIAA Student Member.leeming3@illinois.edu.
†National Defense Science and Engineering Graduate Research Fellow, Aerospace Engineering, AIAA Student Member. aetimm2@illinois.edu.
‡Professor, Aerospace Engineering, Associate AIAA Fellow. rovey@illinois.edu.
§Aerospace Engineer, Spacecraft Engineering Division.michael.mcdonald@nrl.navy.mil

major challenge when implementing molecular propellants in EP systems, as oxygen, water, and air are the molecular propellants that have received the most community interest. To address this problem, recent developments in cathode technology have given rise to Radio Frequency (RF) cathodes. In principle, the RF cathode is an inductively coupled plasma (ICP) source that utilizes electromagnetic induction to generate electrons and produce a plasma. With the use of electric and magnetic fields, electrons can be drawn from the plasma and used as an electron source for EP systems. Due to the lack of thermionic inserts, these cathodes are immune to poisoning, mitigating one of the primary problems of integrating molecular propellants in EP systems [8]

In addition to poisoning, the use of alternative propellants is problematic due to the generation of radical neutrals. Radical neutrals are atomic atoms that have unpaired electrons, making them highly reactive and prone to initiating chemical reactions [9]. The density of radical neutrals has a significant impact on the functionality and longevity of spacecraft and EP systems. When high-energy neutral particles collide with a spacecraft surface or within an EP thruster, they sputter atoms from the material leading to gradual erosion and deterioration [10]. In EP systems, the creation of plasma enhances the propellant mass efficiency. This process simultaneously decreases the number of atomic neutrals present, as detailed in Ref. [1]. Consequently, the density of atomic neutrals in the plasma is a key indicator of the ionization efficiency within the EP system. Additionally, understanding the atomic neutral density aids in predicting and mitigating erosion caused by atomic neutrals. Several methods can be used to determine the atomic neutral density of a plasma. These methods include two-photon absorption laser-induced fluorescence (TALIF), laser spectroscopy (LIF), NO titration, and catalytic probes. However, TALIF, LIF, and NO Titration are time-intensive, expensive, and complex methods that are unable to provide spatially resolved real-time measurements [11]. Catalytic probes, on the other hand, are inexpensive, easy to fabricate, and simple to use in a range of plasma sources [9]. Catalytic probes determine the atomic neutral density of a plasma system by measuring the cooling rate of the catalytic surface after the plasma is shut off. When directly comparing the atomic neutral density measurements made by catalytic probes and methods such as TALIF and NO Titration, past results show that catalytic probes produce similar measurements [11, 12].

Essentially, catalytic probes are disks of metal immersed in plasma. When a catalytic probe is immersed in plasma, the recombination of atomic oxygen into molecular oxygen occurs on the surface of the probe, as seen in Eq. 1.

$$O + O \rightarrow O_2 \tag{1}$$

From recombination events, heat is generated on the surface of the probe, and the probe measures temperatures that are higher than the temperature of the ambient plasma [13]. The schematic of a catalytic probe is shown in Fig. 1. A metal catalytic disk is spot welded to the tip of a stainless-steel K-type chromel-alumel thermocouple. The probe disks are made to be very small, 1-4 mm, to prevent perturbations in the plasma [13]. The probe is encased in alumina to ensure that recombination does not occur on the stainless steel shell of the thermocouple.

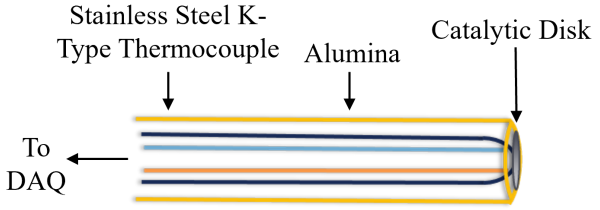

Fig. 1 Schematic of the Catalytic Probe

The probability of a recombination event occurring on the surface of the probe is the recombination coefficient (γ). The recombination coefficient represents the ratio of atoms recombining on the surface to those arriving at the surface per unit time [14]. The method used to describe the recombination event is the Langmuir-Hiselwood mechanism, in which surface recombination of two adsorbed atoms takes place on a catalytic surface [14]. During recombination, two radicals recombine on the catalytic surface and thermal energy is released. Different materials exhibit distinct recombination coefficients in different plasma types [9]. The surface of a catalytic probe is made out of a material, usually a metal, that has a high recombination coefficient for a given plasma. A material with a high recombination coefficient will experience a larger temperature change than one with a lower recombination coefficient [9]. Additionally, metals that tend to form stable oxides are implemented in catalytic probe construction as they ensure that the surface is

optimized for recombination events [12]. Nickel has been utilized extensively as a catalytic surface for determining the atomic neutral oxygen density, n_o, in an oxygen plasma environment, as shown in numerous studies [12, 14, 15]. These investigations used high-purity nickel, with a purity exceeding 99.8%. However, there exists a notable gap in the literature regarding the use of lower purity, and more cost-effective, nickel shims with purity levels below 99.0%.

This investigation implemented catalytic probes to measure the atomic neutral density in an RF plasma source with densities typical for EP-related plasma. The two catalytic probe materials, pure and shim nickel, were chosen to determine the implications of material properties on atomic neutral density measurements. The remainder of this paper is organized as follows: Section II will describe the methodology, experimental setup, testing procedure, and data analysis technique used to determine the atomic neutral density of an RF plasma source. Section III will present the maximum temperature recorded by the catalytic probes, the cooling rates of the probes after plasma shut off, and the atomic oxygen neutral density measured by the probes. Section IV will discuss past literature results for atomic oxygen neutral densities and calculate the dissociation fraction of oxygen. The paper will be concluded in Section V.

II. Methodology

In this study, two nickel catalytic probes and one stainless steel (SS) thermocouple were utilized. The SS thermocouple probe was implemented to approximate the ambient temperature of the plasma and visualize heat due to recombination. The construction of the SS thermocouple probe was identical to that of the nickel probes. Each probe was comprised of a ceramic shield with an outer diameter of 4 mm and a wall thickness of 0.9 mm. The ceramic shield was wrapped around a K-type thermocouple, as shown in Fig. 1, with a diameter of 1.5 mm. The surface of the probes was comprised of 3.2 mm disks that were spot-welded to a 1.6 mm SS thermocouple tip. This study used two types of catalytic probes: one with a disk of 99.99% pure Ni, and another with 98.9% shim Ni. A third disk comprised of 316 SS was implemented for the SS thermocouple probe.

The experimental setup utilized in this investigation is presented in Fig. 2. A water-cooled RF coil, with a diameter of 2.65 mm, was wrapped around a quartz tube with an outer diameter of 55 mm and a thickness of 1.75 mm. Commercial grade O_2 was pumped into the instrumentation cap at 30 SCCM, controlled by two Alicat mass flow controllers. As the gas was fed into the system, the RF coil was powered through a matching network controlled by a Dressler Caesar RF Power Generator. The total pressure of the system was 12 Pa during plasma operation. The three probes were extended into the center of the RF coil, seen in Fig. 2. All three probes were fed through the instrumentation cap and reached the center of the RF coil, 98 mm below the cap. The thermocouple wires, attached to the back of each disk, were connected to an NI USB-6218 Data Acquisition System (DAQ). During experimentation, the temperature of the probes was measured by recording the voltage of each probe.

Before experimentation, the catalytic surfaces were activated. The activation of each probe surface was performed to desorb gases, and possible impurities, that adsorbed to the surface and to form a thin stable layer of oxide on the surface of each probe [14]. To activate the surface, the probes were immersed in 400 W oxygen plasma for 140 sec and cooled down to 300 K. Following catalytic probe activation, the RF generator was turned on for 30 sec. Due to the excessive recombination of oxygen on the surface of the probe, the temperature of the nickel catalytic probes increased above the ambient temperature of the plasma, approximated by the maximum temperature of the SS thermocouple. The maximum temperature of each probe was recorded right after the RF generator was shut off. As the probes cooled, the temperature of each probe was recorded with respect to time until all three probe temperatures reached 300 K. When the temperature of all three probes reached 300 K, the RF was turned back on at increased power. This process was repeated from 10 – 600 W in increments of 50 W. The power was not increased past 600 W because the RF generator had a power limit of 600 W. The cooling rate was determined from the temperatures recorded in the 2 sec immediately following RF shutoff to best approximate the atomic oxygen neutral density [16].

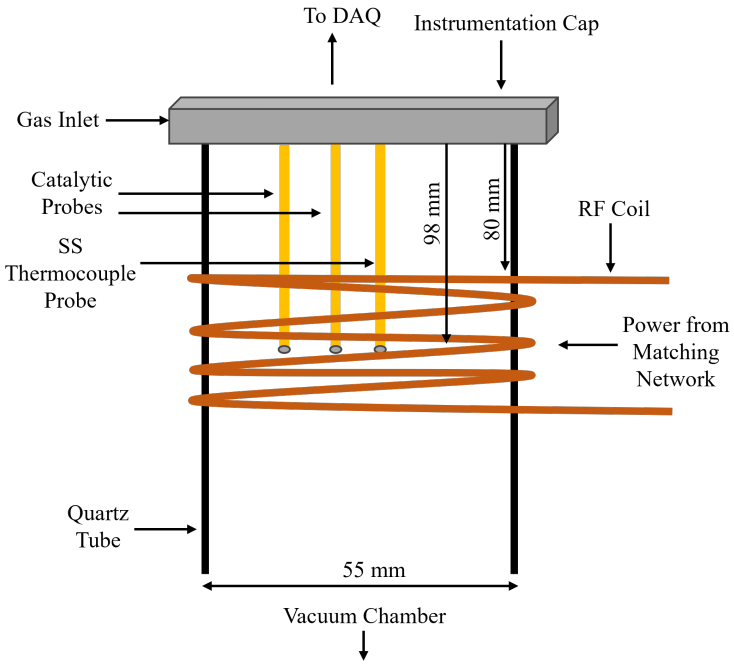

Fig. 2 Schematic of the RF plasma source and experimental apparatus

A. Catalytic Probe Data Analysis

The atomic neutral density in the vicinity of a catalytic probe can be determined based on the cooling rate of the surface immediately following plasma deactivation. During immersion in a plasma, the recombination of atomic oxygen into molecular oxygen occurs on the surface of the probe. When a recombination event occurs, energy, in the form of heat, is released by the reaction. Due to energy dissipation on the catalytic surface, the probe temperature increases above the ambient temperature of the plasma. During plasma immersion, the heating of the nickel disk can be attributed to ion bombardment, electron collisions, and radiation heating, as well as the recombination of oxygen on its surface. The cooling rate is equal to gray body radiation, the thermal conductivity of the gas, and the thermal conductivity of the thermocouple wires [17]. During plasma exposure, the temperature of the probe increases until it reaches a constant temperature, at which point the heating and cooling rates on the surface of the probe are equal [16].

When the plasma is turned off, the heating due to recombination stops as atoms are pumped away or lost to the walls in the vacuum chamber. At that moment, the cooling of the probe is the same as it was during plasma operation. Measuring the cooling rate after plasma turnoff therefore equal to the rate of heating at steady conditions [17]. The atomic neutral density can be derived from the flux of atomic neutral atoms, j, to the probe surface as shown in Eq.2.

$$j = \frac{1}{4} n_o v \tag{2}$$

Here, n_o is the atomic neutral density in the vicinity of the probe, and v is the average thermal velocity of atoms can be defined in Eq 3.

$$v = \sqrt{\frac{8kT_g}{\pi M_o}} \tag{3}$$

Where k is the Boltzmann constant, T_g the temperature of the ambient gas (assumed to be 300 K), and M_o is the mass of an O atom. The heat dissipation rate on the probe by the plasma is determined by the product of the atom flux and their average energy upon surface impact [17]. This heating rate of the probe surface, taking into account heat from recombination, P_h, is defined by Eq. 4.

$$P_h = \frac{1}{2} j \gamma W_{\mathrm{D}} A_p \tag{4}$$

In Eq. 4, W_{D} is the dissociation energy, 4.97×10^{-19} J, and A_p is the surface area of the probe, defined as 2.06×10^{-5} m^{-2} for the pure Ni and 2.01×10^{-5} m^{-2} for the shim Ni, and γ is the recombination coefficient. Just before the plasma turns off, the rate of heating is equal to the rate of cooling. When the power source is turned off, the rate of heating, P_h drops to zero, and the cooling rate, P_c, defined in Eq. 5, remains unchanged. The measured value of the cooling rate is therefore equal to the rate of heating at the constant temperature [18]. The cooling rate of the probe surface, P_c, is defined by Eq. 5.

$$P_c = M C_p \frac{dT}{dt} \tag{5}$$

Here, M is the mass of the probe disk and C_p is the specific heat of the probe material, assumed to be 444 J/(kg K) for both nickel probes. The mass of the pure nickel disk was 1.9×10^{-5} kg and the shim nickel was 1.1×10^{-5} kg. When the plasma is shut off, the cooling rate depends on M, C_p, and the time derivative of the probe temperature $\frac{dT}{dt}$. By equating P_h and P_c, the atomic neutral density in the vicinity of the probe can be determined by Eq. 6.

$$n_o = \frac{4 M C_p}{v \gamma W_D A_p} \frac{dT}{dt} \tag{6}$$

B. The Recombination Coefficient

The recombination coefficient γ is dependent on surface morphology, pressure, and temperature [9]. Previous studies have been conducted to experimentally or computationally determine γ over a range of operational pressures and temperatures for nickel and stainless steel. Each of these studies leveraged a different method to determine the atomic oxygen neutral density in an ICP plasma which can be directly compared to an RF plasma source. In the studies, the determined atomic neutral densities were also used to determine the recombination coefficient. Table 1 includes a literature review conducted by D. Paul, et. al [19]. This literature review details material, pressure, temperature, the method used to determine the neutral density, and the γ value calculated based on these parameters.

In addition to the literature, the materials and operational conditions used in this study are shown in bold in Table 1. The ambient temperature in this evaluation ranged from 300 to 400 K and the ambient pressure was 12 Pa. By comparing these conditions to those of the previous studies, it is reasonable to assume values of γ for Ni. For the nickel catalytic probes used in this study, the recombination coefficient was assumed to be the well-characterized value of 0.27. This is a reasonable assumption because the pressure falls within the 10 to 400 Pa range presented in the 1. The ambient temperature also corresponds well to the range of 300 to 1100 K presented in Table 1. Additionally, in Table 1, the recombination coefficient of oxygen on stainless steel is given. The past literature results show that γ is low and varies greatly with pressure and temperature. In this study, it was assumed that the SS thermocouple probe experienced a temperature increase due to ion bombardment, electron collisions, and radiation heating, and the heat generated by recombination was assumed to be negligible.

Table 1 Literature review of atomic oxygen recombination coefficients and the values used in this study.

Material	γ	P (Pa)	T (K)	Method to Determine n_o	Ref.
Ni	**0.27**	**12**	**300 - 400**	—	
Ni	0.27	10 - 100	500 - 1100	thermocouple probe	[14]
Ni	0.27	10 - 400	800	Langmuir probe + fiber optic catalytic probe	[12]
Ni	0.27	100	550	thermocouple probe + OES + NO titration + Langmuir probe	[20]
Ni	0.28	30 - 280	300	side-arm + fiber optic catalytic probe	[21]
SS	0.17	5	330	neutral mass spectrometry and Langmuir probe	[22]
SS	0.31 - 0.02	1 - 100	400 - 700	TALIF	[23]
SS	0.09	0.2 - 3	300	spinning wall desorption mass spectrometry	[24]
SS	0.09	0.2 - 3	310	Langmuir probe + actinometry + mass spectrometry	[25]
SS	0.07	100	550	thermocouple probe + OES + NO titration + Langmuir probe	[20]

III. Results

When the catalytic and SS thermocouple probes were exposed to the oxygen plasma, the temperature of each probe increased. In this experiment, the SS thermocouple probe was used to verify that recombination events were occurring on the surface of the Ni probes, as the heat due to recombination was assumed to be negligible. It was assumed that the SS thermocouple probe experienced a temperature increase when exposed to plasma due to ion bombardment, electron collisions, and radiation heating. The Ni probes underwent heating from these effects and experienced additional heating due to recombination. Thus, the temperature difference between the Ni catalytic probes and the SS thermocouple can be attributed to recombination heating.

The temperature of the Ni probes increased well above the ambient temperature of the plasma due to catalytic recombination on the surface. As previously detailed in Section II, the temperature of each probe was measured immediately after the plasma shut off. The maximum temperatures reached by the probes, shown in Fig. 3, highlight the heat generated through recombination processes with both of the nickel probes exhibiting higher temperatures than the SS thermocouple probe. The higher temperatures observed in Fig. 3 for the pure Ni probe can be attributed to its greater efficiency in facilitating catalytic recombination and higher mass when compared to the shim probe. The pure Ni probe exhibits temperatures that, on average, are 10% higher than the shim and 19% higher than the SS thermocouple probe across all power levels. This suggests that there may be a difference in recombination between the pure and shim Ni probes. Despite their similar chemical compositions, the difference in temperatures between the pure and shim Ni probes shows that catalytic recombination processes are susceptible to even 1% variations in material purity.

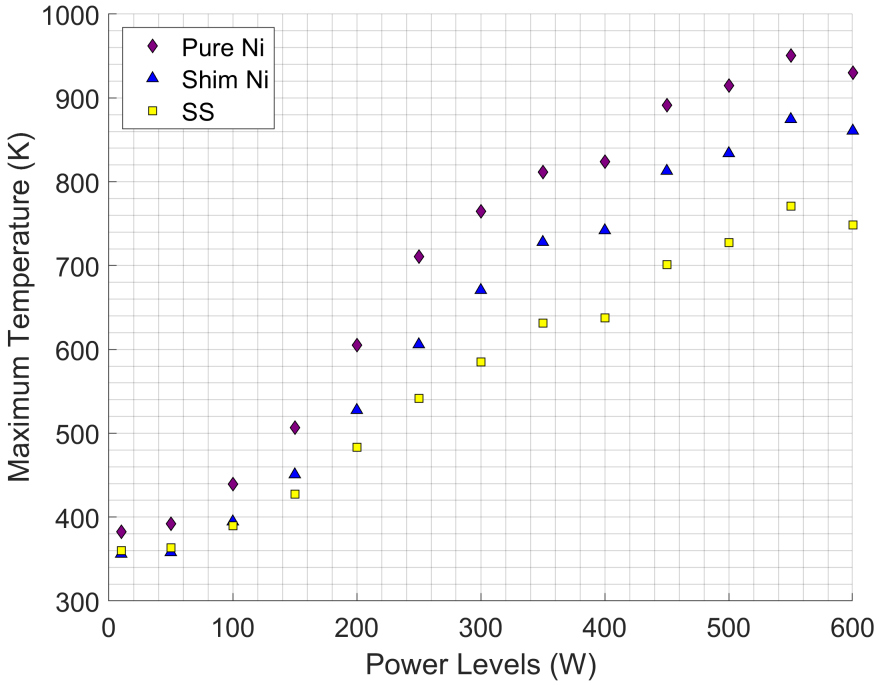

Fig. 3 The maximum temperature recorded by the pure and shim nickel catalytic probes and the SS thermocouple probe

The temperature of the probes measured at plasma shut off, t + 0, and extending to t + 2 sec is plotted with respect to time as shown in Fig. 4. The slope of each line is the cooling rate of the probe. As visualized in Fig.4, the cooling rate displayed linear decreases in temperature from t + 0 sec to t + 2 sec at four distinct power levels: 100, 300, 500, and 600 W. These power levels were chosen as a representation of the trends observed at power levels ranging from 10 to 600 W. The application of linear trend lines to the cooling temperature curves in Fig. 4 reveals a consistent linear relationship between the power levels and probe cooling rate. The linear relationship between cooling rate and power is maintained across all power levels. This trend demonstrates that despite differences in catalytic materials, efficiencies, and thermal conductivity, the fundamental trend of energy absorption and dissipation by the probes is both linear and uniform.

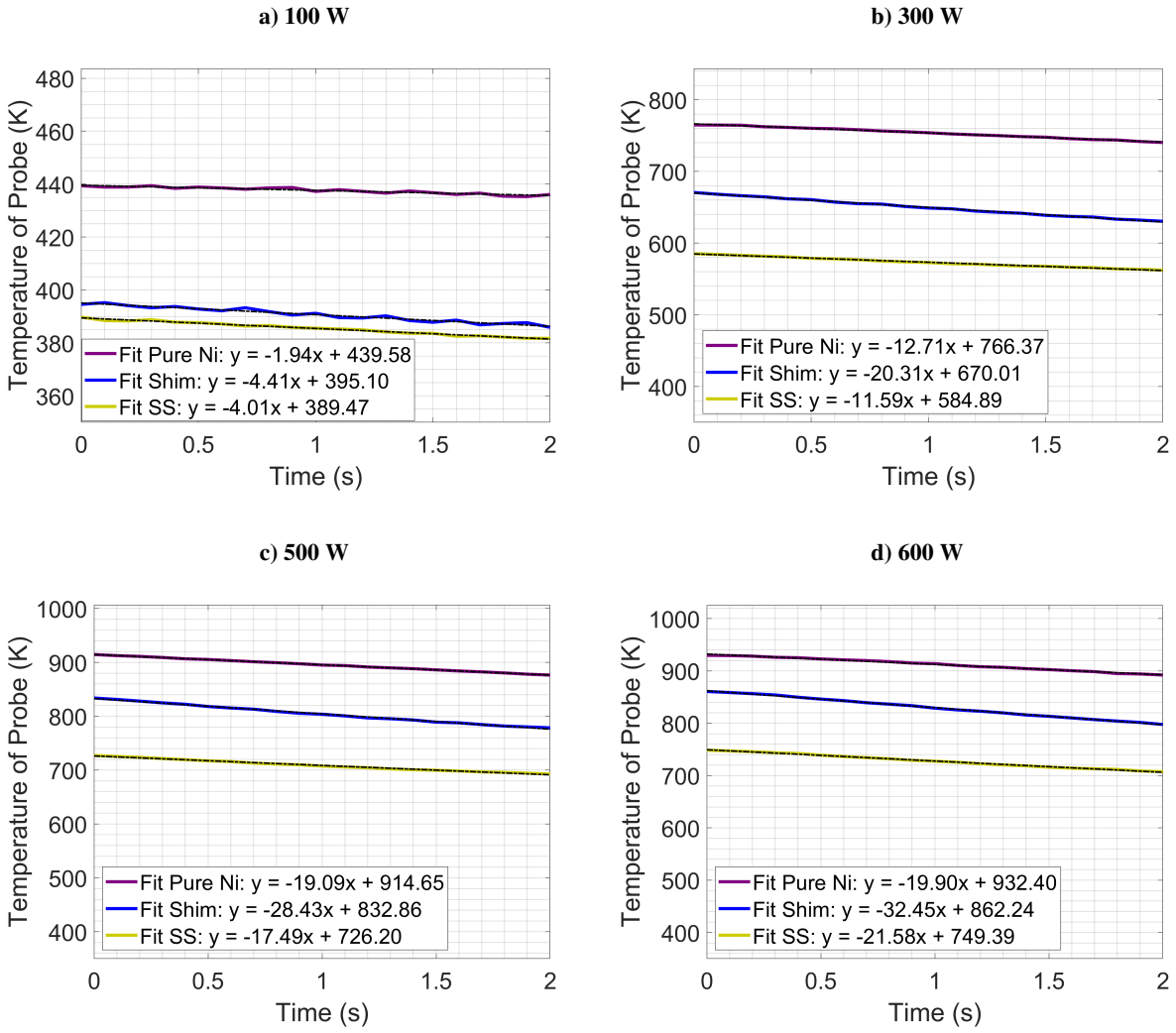

Fig. 4 The temperature curve after 2 s of each of the probes after the plasma shut off at a) 100W, b) 300 W, c) 500 W, and d) 600 W along with the corresponding fitted linear equation

To determine n_o, the cooling rate was recorded for the pure Ni and shim Ni catalytic probes, as seen in Table 2. Additionally, the cooling rate of the SS thermocouple was also recorded. The cooling rate, determined by taking the first derivative of the temperature with respect to time, of the pure Ni probe was 0.58 K/s at the lowest power setting, 10 W, and rose to 19.9 K/s at the highest power, 600 W. The SS probe follows a similar trend, where the initial cooling rate was at 0.06 K/s for 10 W, but exceeded that of the pure Ni at 600 W and reached 21.6 K/s. Most notably, the shim Ni probe displayed the largest increase, starting from a rate of 0.32 K/s at 10 W and ending with a rate of 32.4 K/s at 600 W.

The shim probe exhibited a higher cooling rate than the pure Ni and SS. The higher cooling rate of the shim Ni probe, as compared to the pure Ni, is likely due to shim Ni having a lower mass than pure Ni and its chemical composition. Pure nickel had a measured mass of 1.9 $\times 10^{-5}$ kg and the shim nickel had a measured mass of 1.1 $\times 10^{-5}$ kg. The lower mass of the shim Ni probe could allow it to lose heat more quickly than pure Ni, possibly explaining its higher cooling rate. Additionally, this higher cooling rate could be due to differences in the surface morphology between the catalytic surfaces. The increased surface area due to microstructural features like grain boundaries or surface roughness can enhance the emissivity of the material, allowing it to radiate heat more effectively and thus cool down at a faster rate once the plasma source is turned off.

Table 2 The absolute values of the approximately linear cooling rate, $\frac{dT}{dt}$, for each of the probes 2 sec after plasma turn off.

Power Level (W)	Pure (K/s)	Shim (K/s)	SS (K/s)
10	0.58	0.61	0.42
50	0.83	1.13	1.71
100	1.94	4.41	4.01
150	3.73	8.01	6.11
200	6.03	11.3	7.75
250	10.4	15.7	9.57
300	12.7	20.3	11.6
350	13.7	22.4	12.4
400	15.4	24.4	13.6
450	16.7	27.7	16.7
500	19.1	28.4	17.5
550	20.05	29.4	19.2
600	19.9	32.4	21.6

Figure 5 shows the atomic neutral density of oxygen at the center of an RF plasma source, measured by the pure and shim nickel catalytic probes across power levels ranging from 10 to 600 W. The pure and shim Ni probes measured atomic neutral density values and had an average difference of 18%. This could be due to the lower mass of the shim Ni probe, as the lower mass would allow it to radiate heat faster, as seen in Table 2, thereby affecting the neutral density. Interestingly, though the shim Ni probe had a lower mass and faster cooling rate than the pure Ni, the measured atomic neutral density was still in the range of the pure Ni. During experimentation, it could be seen that there was less oxide on the surface of the shim than the pure Ni. This indicated a difference in the recombination events occurring on the surface of each probe and that a more refined recombination coefficient that reflects these differences should be utilized in future experiments.

Additionally, Fig. 5 displays the average atomic neutral density calculated by averaging the neutral densities determined by the two catalytic probes. As the power level increased from 10 to 600 W, the average atomic neutral density increased from 6.1×10^{18} m^{-3} to 3.8×10^{20} m^{-3} respectively. This relatively linear increase, suggests a proportional relationship between the power supplied to the system and the density of neutral species generated within the plasma. The rise in atomic oxygen neutral density as the power increases can be attributed primarily to increased ionization and excitation processes, driven by the higher energy input at elevated power levels. In the plasma, a higher power input correlates with an increased rate of neutral species generation. This phenomenon is evident from the increasing atomic neutral density with power observed by catalytic probes in this experiment [26–28].

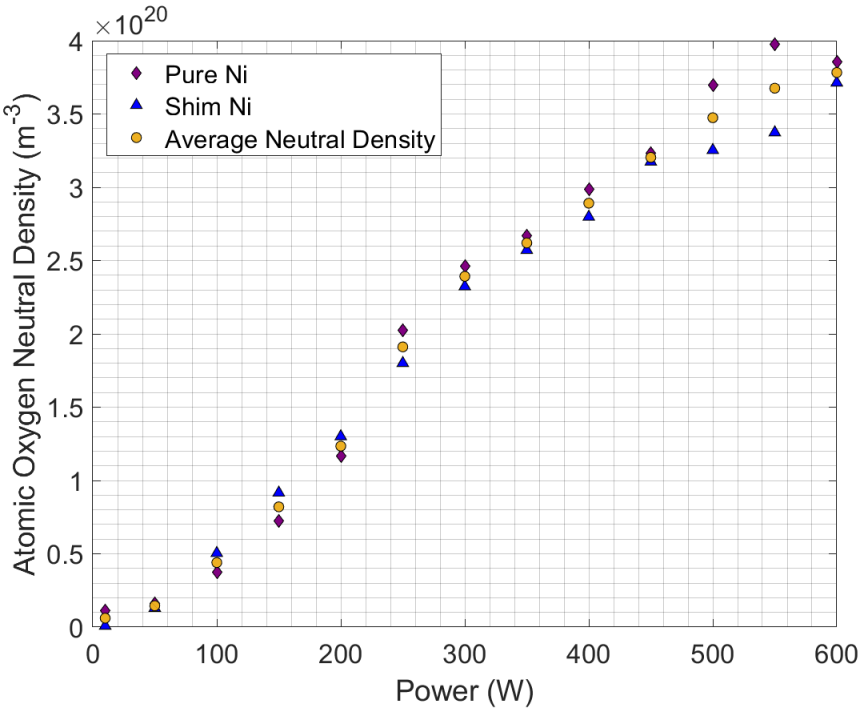

Fig. 5 The average of the atomic neutral density from the pure and shim nickel catalytic probes at the center of the RF plasma source along with the average calculated atomic neutral density

IV. Discussion

In this study, the average atomic oxygen neutral density ranged from 6.1×10^{18} m^{-3} to 3.8×10^{20} m^{-3} aligning with prior research on oxygen ICP plasma sources. As shown in Table 3, the previous studies measured the atomic neutral density by using nickel catalytic probes in ICP sources. Cvelbar et al. [12] reported densities around 1×10^{20} m^{-3} at 300 W and 10 Pa. At lower power settings of 200 W, and pressures of 10 and 20 Pa, the densities were found to be 6×10^{20} m^{-3} and 2×10^{21} m^{-3}, respectively [14]. Additionally, at 30 W and 10 Pa, M. Mozetic et al. [15] reported that the atomic oxygen density was 3×10^{20} m^{-3}. The similarity in experimental conditions and results with previous studies inspires confidence in the measurements made in this study.

Table 3 Comparison of atomic oxygen neutral density values from this study with previous Literature in ICP sources.

Power (W)	Catalytic Material	Pressure (Pa)	Atomic Oxygen Neutral Density (m^{-3})	Ref
10 - 600	**Ni**	**12**	**6.1×10^{18} m^{-3} to 3.8×10^{20} m^{-3}**	This Study
300	Ni	10 - 400	1×10^{20} to 7×10^{21}	[12]
-	Ni	10 - 100	3×10^{19} to 2×10^{21}	[18]
200	Ni	10 - 20	6×10^{20} to 2×10^{21}	[14]
30 - 140	Ni	10	8×10^{20} to 3.5×10^{21}	[15]

To further verify the measured atomic neutral density, the dissociation fraction of the oxygen plasma was estimated. The dissociation fraction represents the ratio of oxygen molecules that have split into atomic atoms to the total number of oxygen molecules. By utilizing the atomic neutral density of oxygen, determined by the pure nickel catalytic probe, the dissociation fraction can be calculated [14, 17]. The plasma was assumed to be in an equilibrium state therefore the ideal gas law could be applied. Based on this assumption, the dissociation fraction can be calculated using Eq. 7.

$$n_D = \frac{n_o k T_w}{2P} \tag{7}$$

In Eq. 7, T_w represents the temperature of the vacuum wall, assumed to be 300 K, and n_o is the atomic neutral density measured by the pure nickel catalytic probe. The factor of 1/2 is implemented to account for the two atoms in an oxygen molecule that, when dissociated, yield two oxygen atoms. As seen in Fig. 6 the dissociation of oxygen fraction exhibits a clear upward trend as power increases. The dissociation fraction increases from 1% to just under 7% at 600 W. These results correspond with past literature values, which have found that the average dissociation fraction of oxygen at low pressure ranges from 1-10% [17, 29]. The estimated dissociation fraction and the alignment with literature values inspire confidence in the accuracy of the measurements made by the catalytic probes. Additionally, the increasing trend over the power levels suggests a power dependency in the plasma's capacity to dissociate oxygen molecules.

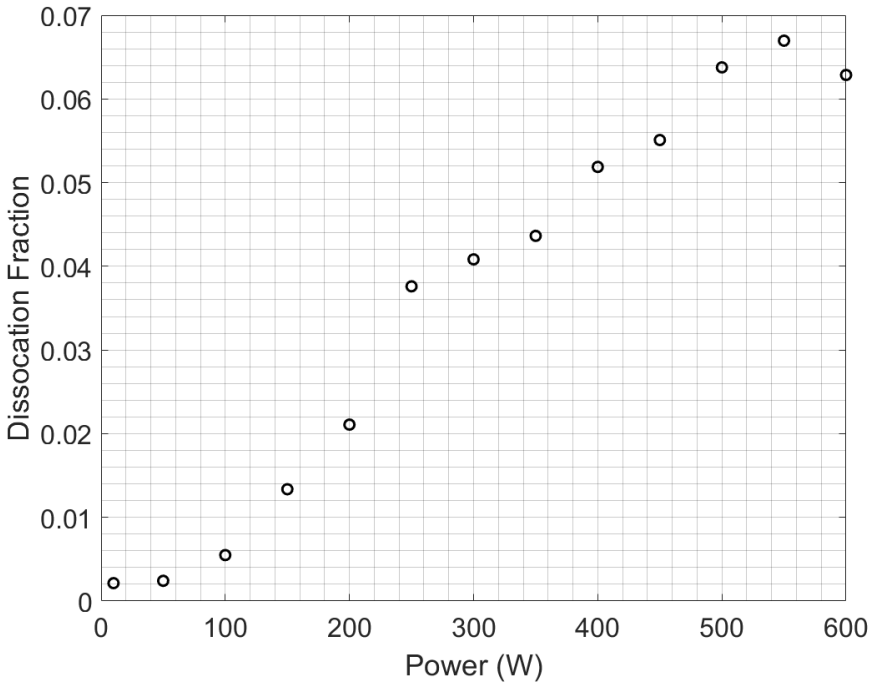

Fig. 6 Dissociation fraction of oxygen calculated from the measurements of atomic neutral density made by the pure Ni catalytic probe

V. Conclusion

This investigation implemented a series of nickel catalytic probes to measure the atomic oxygen neutral density inside an RF plasma with densities typical of an EP-related plasma. It was shown that the average atomic oxygen density in an RF plasma source increased across a power range of 10 to 600 W, from 6.1×10^{18} m^{-3} to 3.8×10^{20} m^{-3}, respectively. The results reveal an 18% difference between the atomic oxygen neutral density measured by the pure and shim nickel. The findings suggest a sensitivity of catalytic recombination to material properties, indicating that minor variations in purity could influence the recombination rate and probe temperature. Based on this investigation, nickel catalytic probes are promising for implementation in future molecular propellant EP plasma devices to characterize the atomic oxygen neutral density of the plasma. This study not only provides a foundation for future studies into atomic oxygen neutral densities but demonstrates a promising approach to measuring atomic oxygen neutral densities in EP systems.

VI. Acknowledgements

This study was completed at the Naval Research Laboratory. We extend our profound gratitude to Marcel Gerogin, Nolan Uchizono, and Mitchell Paul for their unwavering support, invaluable insights, and dedicated mentorship, which were instrumental in every phase of this project.

Further, we offer heartfelt thanks to the Naval Research Laboratory summer interns, Douglas Adams, Hannah Hutton, and Jacob Freeze. Their perceptive contributions and steadfast collaborative spirit significantly enriched the depth and quality of this study.

Funding Sources

This research was sponsored by the Office of Naval Research (ONR) Naval Research Enterprise Internship Program (NREIP) and the Air Force Office of Scientific Research through grant AFFA9550-23-1-0025.

References

[1] Goebel, D. M., and Katz, I., *Fundamentals of Electric Propulsion: Ion and Hall Thrusters*, John Wiley & Sons, 2008.

[2] Tirila, V.-G., Demarie, A., and Ryan, N. C., "Review of alternative propellants in Hall Thrusters," *Acta Astronautica*, 2023. https://doi.org/10.1016/j.actaastro.2023.07.047.

[3] Taccogna, F., Cichocki, F., and Minelli, P., "Coupling plasma physics and chemistry in the PIC model of electric propulsion: Application to an air-breathing, low-power Hall thruster," *Frontiers in Physics*, 2022, pp. 1–19. https://doi.org/https://doi.org/10.3389/fphy.2022.1006994.

[4] Rafalskyi, D., Martínez, J. M., Habl, L., Rossi, E. Z., Proynov, P. P., Boré, A., Baret, T., Poyet, A., Lafleur, T., Dudin, S., and Aanesland, A., "In-orbit demonstration of an iodine electric propulsion system," *Nature*, Vol. 599, 2021, pp. 411 – 415. https://doi.org/10.1038/s41586-021-04015-y.

[5] Oh, D. Y., Collins, S., Drain, T., Hart, W., Imken, T., Larson, K., Marsh, D., Muthulingam, D., Snyder, J. S., and Trofimov, D., "Development of the Psyche mission for NASA's discovery program," *36th International Electric Propulsion Conference*, Vienna, Austria, 2019, pp. 1–29.

[6] Gallagher, H. E., "Poisoning of LaB6 Cathodes," *Journal of Applied Physics*, Vol. 40, No. 1, 2003, pp. 44–51. https://doi.org/10.1063/1.1657092.

[7] Becatti, G., and Goebel, D. M., "500-A LaB6 Hollow cathode for high power electric thrusters," *Vacuum*, Vol. 198, 2022, p. 110895. https://doi.org/10.1016/j.vacuum.2022.110895.

[8] Georgin, M. P., McDonald, M. S., and Brooks, J. W., "Theory of RF Plasma Cathodes and Supporting Experiments for Electric Propulsion Applications," *AIAA SCITECH 2023 Forum*, American Institute of Aeronautics and Astronautics, National Harbor, MD, 2023. https://doi.org/10.2514/6.2023-0844.

[9] Qerimi, D., Panici, G., Jain, A., Jacobson, D., and Ruzic, D. N., "Determination of recombination coefficients for hydrogen, oxygen, and nitrogen gases via in situ radical probe system," *Journal of Vaccum Science and Technology A*, Vol. 39, 2000. https://doi.org/10.1116/6.0000787.

[10] Iwamoto, M., Yananoto, N., Morita, T., Nakashima, H., Tomita, K., and Uchino, K., "Rayleigh Scattering Measurement of Neutral Atom Number Density Downstream of a Hall Thruster under Cold Flow Conditions," *Translated Japan Society of Aerospace Space Science*, Vol. 60, No. 5, 2017, pp. 327, 330. https://doi.org/10.2322/tjsass.60.327.

[11] Gaboriau, F., Cvelbar, U., Mozetic, M., Erradi, A., and Rouffet, B., "Comparison of TALIF and catalytic probes for the determination of nitrogen atom density in a nitrogen plasma afterglow," *Journal of Physics D: Applied Physics*, Vol. 42, No. 5, 2009, p. 055204. https://doi.org/10.1088/0022-3727/42/5/055204.

[12] Cvelbar, U., Mozetič, M., and Ricard, A., "Characterization of oxygen plasma with a fiber optic catalytic probe and determination of recombination coefficients," *IEEE Trans. Plasma Sci.*, Vol. 33, 2005, pp. 834–837. https://doi.org/10.1109/TPS.2005.845286.

[13] Mozetic, M., Cvelbar, U., Vesel, A., and et al., "A diagnostic method for real-time measurements of the density of nitrogen atoms in the postglow of an Ar - N2 discharge using a catalytic probe," *Journal of Applied Physics*, Vol. 97, No. 103308, 2005. https://doi.org/10.1063/1.1906290.

[14] Sorli, I., and Rocak, R., "Determination of atomic oxygen density with a nickel catalytic probe," *Journal of Vacuum Science and Technology A*, Vol. 18, No. 11, 2000, pp. 338, 342. https://doi.org/10.1116/1.52189.

[15] Mozetic, M., "Characterization of reactive plasmas with catalytic probes," *Surface & Coatings Technology*, Vol. 201, 2007, pp. 4837–4842. https://doi.org/10.1016/j.surfcoat.2006.07.031.

[16] R. Zaplotnik, M. M., A. Vesel, "A Fiber Optic Catalytic Sensor for Neutral Atom Measurements in Oxygen Plasma," *Senors*, 2012. https://doi.org/10.3390/s120403857.

[17] Mozetič, M., Vesel, A., Gaillard, M., et al., "Atomic Oxygen Concentration in a Flowing Post-Discharge Reactor," *Plasmas and Polymers*, Vol. 6, 2001, pp. 71–79. https://doi.org/10.1023/A:1011305020613.

[18] Mozetic, M., and Zalar, A., "Recombination of neutral oxygen atoms on stainless steel surface," *Applied Surface Science*, Vol. 158, 2000. https://doi.org/10.1016/S0169-4332(00)00007-6.

[19] Paul, D., Mozetic, M., Zaplotnik, R., Primc, G., Donlagic, D., and Vesel, A., "A Review of Recombination Coefficients of Neutral Oxygen Atoms for Various Materials," *Materials*, Vol. 16, No. 1774, 2023. https://doi.org/10.3390/mal16051774.

[20] Mozetič, M., and Cvelbar, U., "Heterogeneous recombination of O atoms on metal surfaces," *Int. J. Nanosci.*, Vol. 6, 2007, pp. 121–124. https://doi.org/10.1142/S0219581X07004365.

[21] Drenik, A., "The Probability of Heterogeneous Recombination of Hydrogen and Oxygen Atoms on the Surfaces of Fusion-Relevant Materials," Ph.D. thesis, Jožef Stefan International Postgraduate School, Ljubljana, Slovenia, 2009.

[22] Singh, H., Coburn, J., and Graves, D., "Recombination coefficients of O and N radicals on stainless steel," *J. Appl. Phys.*, Vol. 88, 2000, pp. 3748–3755. https://doi.org/10.1063/1.1289046.

[23] Gomez, S., Steen, P. G., and Graham, W. G., "Atomic oxygen surface loss coefficient measurements in a capacitive/inductive radio-frequency plasma," *Applied Physics Letters*, Vol. 81, No. 1, 2002, pp. 19–21. https://doi.org/10.1063/1.1490630.

[24] Stafford, L., Guha, J., and Donnelly, V., "Recombination probability of oxygen atoms on dynamic stainless steel surfaces in inductively coupled O2 plasmas," *J. Vac. Sci. Technol. A Vac. Surf. Film.*, Vol. 26, 2008, pp. 455–461. https://doi.org/10.1116/1.2902953.

[25] Stafford, L., Guha, J., Khare, R., Mattei, S., Boudreault, O., Clain, B., and Donnelly, V., "Experimental and modeling study of O and Cl atoms surface recombination reactions in O2 and Cl2 plasmas," *Pure Appl. Chem.*, Vol. 82, 2010, pp. 1301–1315. https://doi.org/10.1351/pac-con-09-11-02.

[26] Saloum, S., Naddaf, M., and Alkhaled, B., "Active species characterization in RF remote oxygen plasma using actinometry OES and electrical probes," *Vacuum*, Vol. 85, No. 3, 2010, pp. 439–442. https://doi.org/10.1016/j.vacuum.2010.08.007.

[27] He, J., and Zhang, Y. T., "Modeling Study on the Generation of Reactive Oxygen Species in Atmospheric Radio-Frequency Helium–Oxygen Discharges," *Plasma Processes and Polymers*, Vol. 9, 2012, pp. 919–928. https://doi.org/10.1002/ppap.201200067.

[28] Dedrick, J., Schröter, S., Niemi, K., Wijaikhum, A., Wagenaars, E., de Oliveira, N., Nahon, L., Booth, J. P., O'Connell, D., and Gans, T., "Controlled production of atomic oxygen and nitrogen in a pulsed radio-frequency atmospheric-pressure plasma," *Journal of Physics D: Applied Physics*, Vol. 50, No. 45, 2017, p. 455204. https://doi.org/10.1088/1361-6463/aa8da2.

[29] Kocian, P., "NOTE ON THE DISSOCIATION OF OXYGEN IN A LOW-PRESSURE DISCHARGE PLASMA," *Physics Letters*, Vol. 73a, No. 1, 1979. https://doi.org/10.1016/0375-9601(79)90736-9.